RSC Advances

Effect of bromide ions on the corrosion behavior of hafnium in anhydrous ethanol

Journal:	*RSC Advances*
Manuscript ID:	RA-ART-02-2015-002233.R1
Article Type:	Paper
Date Submitted by the Author:	20-Mar-2015
Complete List of Authors:	Wang, Changhong; Central South University, School of Metallurgy and Environment Yang, Shenghai; Central South University, School of Metallurgy and Environment Chen, Yongming; Central South University, School of Metallurgy and Environment Wang, Biao; Central South University, School of Metallurgy and Environment He, Jing; Central South University, School of Metallurgy and Environment Tang, Chaobo; Central South University, School of Metallurgy and Environment

SCHOLARONE™
Manuscripts

Effect of bromide ions on the corrosion behavior of hafnium in anhydrous ethanol

Changhong Wang, Shenghai Yang,* Yongming Chen, Biao Wang, Jing He and Chaobo Tang

School of Metallurgy and Environment, Central South University, Changsha 410083, China

Abstraction: The electrochemical behaviors of hafnium (Hf) in Et_4NBr ethanol solutions were investigated using cyclic voltammetry, potentiodynamic polarization, chronoamperometry, impedance and SEM techniques. The potentiodynamic anodic polarization curves did not exhibit an active dissolution region near corrosion potential due to the presence of an oxide film on the electrode surface, which was followed by pitting corrosion as a result of the passivity breakdown by the aggressive attack of bromide ion (Br^-). The pitting potential (E_b) shifted to more noble values with increasing scanning rate, but in a more negative direction with increasing solution temperature and Br^- concentration. The apparent activation energy was calculated as 27.074 kJ mol^{-1} by the Tafel extrapolation. The current/time transients indicated that the incubation time for passivity breakdown decreased slightly with increasing Br^- concentration and applied positive potential. The impedance spectra exhibited that the resistance of the passive layer and charge transfer decreased with an increase in Br^- concentration and applied positive potential, while the resistance of the solution was nearly constant with increasing applied positive potential and decreased with increasing Br^- concentration. The Hf surface morphology and the growth of pitting process were studied by SEM techniques and its images confirmed the existence of pits on the Hf surface.
Key words: anhydrous ethanol; electrochemical behavior; hafnium; pitting corrosion; Et_4NBr

1. Introduction

The silicon-based microelectronics industry steadily advanced the integrated circuit technology in accordance with Moore's famous law to meet the continuously raising demands regarding size, power consumption, and many other characteristics of state-of-the-art complementary metal-oxide-semiconductors.[1,2] As the semiconductor industry ushered in nanometer era,[3] a gate dielectric thickness in the field effect transistor (FET) reached its physical limits because of an increase in leakage currents due to tunneling effects.[2] Have the very good times gone with it? Fortunately, in such urgent time a solution has been proposed, which involves replacing the well known universal gate dielectric, SiO_2, by new materials with higher permittivities.[4] Significant attention has been paid to IV-B metal oxides, among which HfO_2 is considered the most promising due to its large bandgap (5.5-6.0), relatively high dielectric constant (22-25), high breakdown field (3.9-6.7 MV cm^{-1}), high thermal stability and large heat of formation (À271 kcal mol^{-1}).[5] For these reasons, it has become a hot spot. As reported by the IBM Corporation in 2007, the first working 45-nm microprocessor consisting of 410 million transistors, which is called the Penryn dual-core microprocessor and made by the atomic-layer deposition (ALD) method, is manufactured mainly by replacing SiO_2 with hafnium-based oxides.[6]

There are many precursors of hafnium oxide, including $HfCl_4$,[7] $Hf(NEtMe)_4$,[8] $Hf(Cp)_4$,[9] hafnium acetylacetone, hafnium metallocene,[10] $Hf(O-iPr)_4$[11] and $Hf(O^nBu)_4$[12]. Hafnium halides, metal alkyl organics, ketone salts and chelates of ketone salts[13] are generally solid at room temperature and evaporate at a nonuniform rate when heated to sublimation. Me-N-R compounds easily decompose in the air as a result of their generally unstable nature. Hafnium alkoxides are liquids at low temperature and have suitable volatilization and decomposition temperatures. Therefore, hafnium alkoxides are widely utilized precursors for the ALD of a hafnium oxide layer.

The most common method of preparing metal alkoxides is based on the halide synthesis.[14] This method has multistep processes, and the starting materials are difficult of access. In addition, it involves various by-processes

which contaminate the products and decrease their yields.[15] On the other hand, the direct electrochemical synthesis of metal alkoxides has such advantages as a short process, less by-products, high productivity and no waste pollution. Thus, the direct electrochemical synthesis of metal alkoxides by anode dissolution of metals in absolute alcohols in the presence of a conductive admixture seems a very promising method. For example, during the electrosynthesis of tantalum ethoxide, the recovery ratio of tantalum could reach 90.25%.[16] In addition, the anodic oxidation of Hf in anhydrous alcohols in the presence of LiCl as a conductive additive was carried out to give quantitative yields. The products were proven by means of chemical analysis, X-ray powder, and IR spectral studies.[17] Apart from some studies on the electrochemical synthesis of hafnium alkoxides, to the author's knowledge, few reports have related to the electrochemical behavior of the electrosynthesis of hafnium alkoxides.[18-21] In the present study, the electrochemical behavior of Hf was investigated in anhydrous ethanol containing supporting electrolytes using potentiodynamic polarization, cyclic voltammetry, chronoamperometry, impedance and SEM techniques, which are instrumental in understanding the reaction mechanism.

2. Experimental

Anhydrous ethanol was supplied by Tianjing Hengxing Chemical Preparation Corporation. Et_4NBr was purchased from Sinopharm Chemical Reagent Corporation Limited. The working electrode employed was made from a very pure Hf rod (99.9%), which was supplied by the Northwest Institute for Non-ferrous Metal Research. The electrode used was cut as cylindrical rods and mounted into glass tubes using Araldite to offer an active flat disc shaped surface of 4.29 mm^2 geometric area to be immersed in the testing solution. Prior to each experiment, the electrode was successively polished with a series of emery papers from a coarse grade of 1200 to fine grade of 3500. The electrode was then rinsed with ethanol and finally dipped in the electrolytic cell.

The experiments were carried out in a 250 mL volume glass electrolytic cell using Pt foils of 1 cm × 1 cm and 2 cm × 2 cm geometric areas as auxiliary and reference electrodes, respectively. Electrochemical measurements were performed using a potentiostat/galvanostat (CHI660C Electrochemical Workstation provided by Shanghai CH Instrument Company, China) connected to a personal computer. All chemicals used were of analytically pure grade. The electrolyte solutions were prepared from anhydrous ethanol and tetraethylammonium bromide (Et_4NBr). Prior to the experiments, the solutions were deaerated with N_2 for 30 min to remove O_2 dissolved in the solution.

The basic experimental conditions were anhydrous ethanol 250 mL, Et_4NBr 0.06 M and room temperature (30 ± 1 °C). The sample was immersed in the solution until the potential reached a stable value (less than 1.0 mV change over 5 min [22, 23]), and then each measurement was conducted. To investigate the corrosion behavior, cyclic voltammetric measurements were carried out by sweeping linearly the potential from -1 V more negative than the open circuit potential (E_{ocp}) in the positive direction at a given scan rate up to the required potential value, reversing with the same scan rate to the lowest potential, and finally returning to the starting potential to form one complete cycle. To study the influences of the scanning rate (5, 20, 50, 70, 100 mV s^{-1}) on the electrochemical dissolution, potentiodynamic polarization curves were measured from -1 V more negative than E_{ocp} to 4 V at the given scan rate. To obtain the effect of the temperature (20, 30, 40, 50, 60 °C), potentiodynamic polarization curves were measured from -1 V to 4 V at the desired scan rate. To investigate the effect of the Et_4NBr concentration (0.02, 0.04, 0.06, 0.08, 0.10 M), potentiodynamic polarization measurements were carried out from -1 V to 4 V, the chronoamperometry was recorded for 80 s at a constant potential of 2.5 V, and the electrochemical impedance was measured using AC signals of amplitude 5 mV in the frequency range from 0.1 Hz up to 0.1 MHz. To investigate the effect of the electrode potentials (0.4, 0.8, 1.2, 1.6, 2.0, 2.8, 3.2 V), chronoamperometry measurements were recorded for 200 s at a constant anodic potential E_a, and the electrochemical impedance was measured. The frequency range analyzed went from 0.1 Hz up to 0.1 MHz. SEM techniques were adopted to study the Hf surface after anodization at 2.5 V for 3 min in anhydrous ethanol containing different Et_4NBr concentrations (0.02, 0.06,

0.10 M). Each test was repeated at least three times to confirm reproducibility.

3. Results and Discussion

3.1 Determination of the scanning range

Fig. 1 shows a wide scanning-range cyclic voltammogram of Hf starting from -1 V and reversed at various positive potentials ($E_{s, a}$) in anhydrous ethanol containing 0.08 M Et$_4$NBr with a scanning rate of 50 mV s^{-1}. Because this thesis mainly discusses the electrochemical dissolution mechanism of Hf, the scanning range was chosen within the anode polarization region. It is clear that increasing the $E_{s, a}$ produces a more pronounced hysteresis loop. When $E_{s, a}$ are reversed at 1 V and 2 V, the cyclic voltammogram of Hf can be hardly observed, and the maximal current densities just rise to 0.159 and 0.815 mA cm^{-2}, respectively, without any sign of the hysteresis loop. When $E_{s, a}$ is reversed at 3 V, a very small hysteresis loop occurs with an anodic peak in the flyback curve, and the maximal current density reaches 2.421 mA cm^{-2}. However, when $E_{s, a}$ are reversed at potentials exceeding 4 V, the shape of the cyclic voltammogram remains almost the same, with a clearly larger hysteresis loop but a gradually diminished anodic peak. Based on both the electrochemical synthesis and current density in the cyclic voltammetry curve, it is suitable to choose the reversed potential as 4 V.
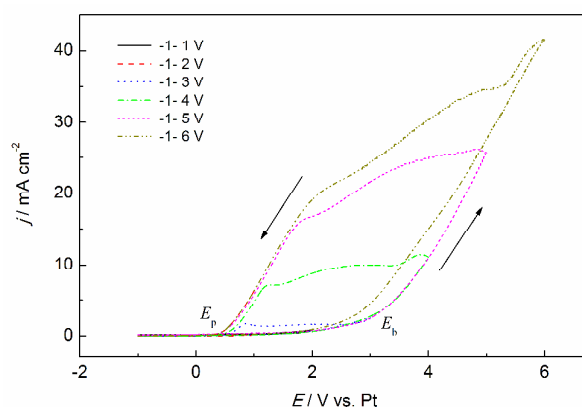

Fig. 1 Cyclic voltammogram of Hf in anhydrous ethanol starting from -1 V and reversed at various positive potentials.

For the cyclic voltammogram ranging from -1 V to 4 V on the positive-going scan, the current density is almost zero. Subsequently, the anodic excursion span does not exhibit an active dissolution region near corrosion potential, and the lack of the active dissolution region can be attributed to the spontaneous passivation of Hf due to the presence of an oxide film on the electrode surface. With the increase of the anodic potential, the current density increases gradually, which can be explained in terms of the chemical dissolution of the oxide film by Br$^-$ ions. However, when the anodic potential exceeds an important value E_b, the current density rises up suddenly, without any sign of gas release, corresponding to the breakdown of the passive film and the initiation and growth of pitting corrosion. After the potential sweep reversal from 4 V, the current density goes up still due to the autocatalytic character of pitting.[24] Afterwards, the current density begins to decline until a platform and an anodic peak appear, which may be attributed to the oxidization of the intermediates produced and absorbed on the Hf surface.[25] As a result, the flyback curve intersects the forward scanning curve at the protection potential E_p. This suggests that the surface of the Hf returns again to the passivated state. Accordingly, a hysteresis loop is clearly obtained, a crucial characteristic of the pitting corrosion phenomenon.[26]

3.2 Influence of potential scanning rate

Fig. 2 illustrates the effect of the potential scanning rate on the anodic polarization curves of Hf in anhydrous ethanol with 0.06 M Et$_4$NBr. It is observed that E_b shifts to more positive values with increasing the scanning rate. This can be explained by the incubation time[27], which is critical to form the passive film breakdown. Increasing the sweep rate corresponds to less time to form a soluble complex at a certain potential. As a result, the passive film is not rapidly dissolved, resulting in the formation of a thicker passive layer. It is interesting to note that the more noble the potential, the shorter the incubation time, which leads to pit growth. Consequently, for a higher scanning rate, pitting initiation appears only at more positive potentials, corresponding to a sufficiently short pit incubation time.[27]
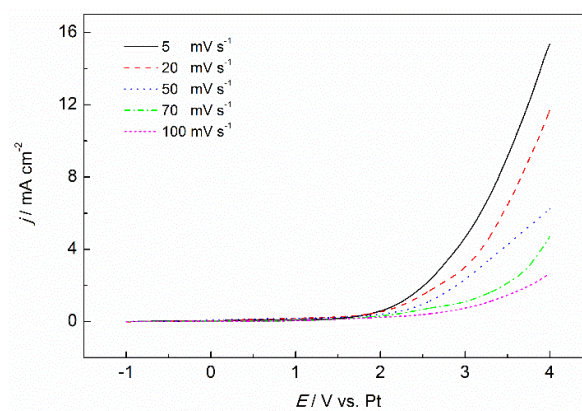

Fig. 2 Potentiodynamic anodic polarization curves of Hf in anhydrous ethanol with different scan rates.

3.3 Influence of temperature

Fig. 3 displays the effect of the temperature on the anodic polarization curves of Hf in a 0.06 M Et$_4$NBr solution of anhydrous ethanol at a scanning rate of 50 mV s^{-1}. As the temperature is increased, E_b shifts to more negative values, indicating a decreased resistance to pitting. It is likely that Br$^-$ ions chemisorb on the surface of Hf,[28] and the increasing temperature may enhance this adsorption.[29] In addition, increasing the temperature facilitates the dissolution of the passive film.[26]

To obtain the apparent activation energy for the corrosion process, the Tafel curves of different temperatures are made, as presented in Fig. 4. The shape and evolution of each curve look similar, indicating that the dissolution mechanisms do not change radically. It is worth noting that increasing the temperature increases the current density, suggesting that a higher temperature is more apt to induce the corrosion of Hf. As is well known, the corrosion current density is a parameter that represents the corrosion rate of a material. The apparent activation energy (E_a) of Hf in a 0.06 M Et$_4$NBr solution of anhydrous ethanol can be calculated from the Arrhenius equation:[30]

$$\lg j_{corr} = \frac{-E_a}{2.303RT} + A \tag{1}$$

where j_{corr} represents the corrosion current density calculated by the Tafel extrapolation, T represents the absolute temperature, R represents the universal gas constant and A represents a pre-exponential factor. A plot of $\lg j_{corr}$ vs T^{-1} presents a straight line (correlation coefficient of 0.995), and the value of E_a obtained from the slope of the straight line is as high as 27.074 kJ mol^{-1}.
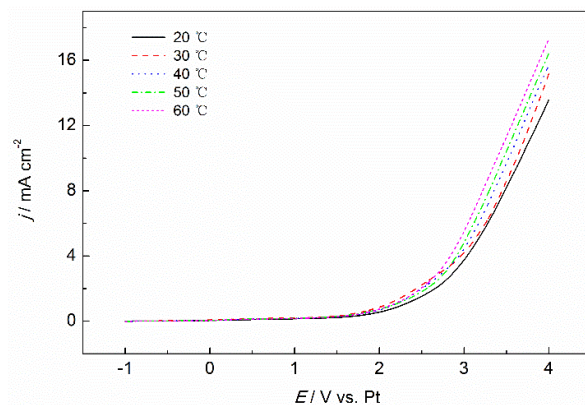
Fig. 3 Potentiodynamic anodic polarization curves recorded for Hf in anhydrous ethanol with different temperatures.
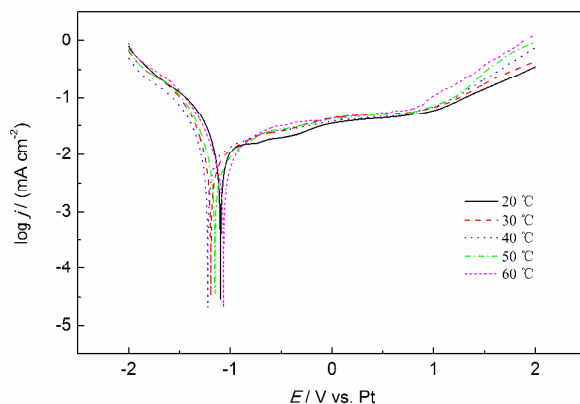

Fig. 4 Tafel curves recorded for Hf in anhydrous ethanol containing 0.06 M Et$_4$NBr at different temperatures with a scan rate of 10 mV s^{-1}.

3.4 Influence of Et$_4$NBr concentration

Fig. 5 presents the influence of various Et$_4$NBr concentrations on the anodic potentiodynamic polarization curves of Hf with a scanning rate of 50 mV s^{-1}. As displayed in Fig. 5, E_b shifts in a more negative direction with an increase in Br$^-$ ions concentration from 0.02 M to 0.10 M. Meanwhile, the current density rises from 7.873 mA cm^{-2} to 15.502 mA cm^{-2} at 4 V, indicating an increased susceptibility to pitting. These behaviors might be due to the weakening of the passive film as a result of the competition among its formation, the formation of the soluble intermediate and the increase of the number of aggressive Br$^-$ ions that attack the passive layer. [31]
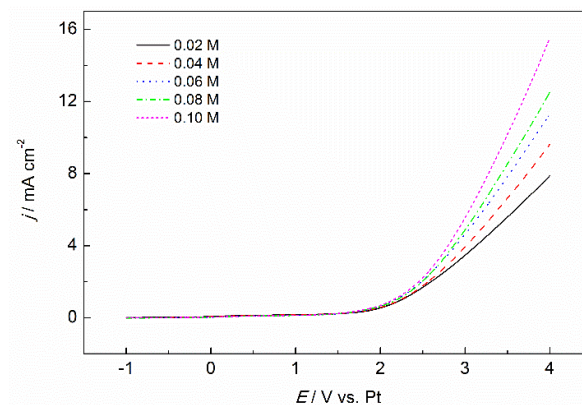
Fig. 5 Potentiodynamic anodic polarization curves recorded for Hf in anhydrous ethanol with different Et₄NBr concentrations.

Fig. 6 presents the potentiostatic current-time transients for Hf in various Et₄NBr concentrations solution of anhydrous ethanol at a constant potential of 2.5 V. As shown in Fig. 6, the current density initially decreases to a minimum value at a certain incubation time (t_i), and t_i decreases with the increase of the Br⁻ ions concentration, indicating that pitting corrosion is more apt to be induced in higher Br⁻ concentrations. These behaviors may be due to the competition between the growth of the oxide films and the dissolution of the passive layer under attack by aggressive Br⁻ ions. After t_i, the current density gradually rises steadily until a steady-state current is attained. The steep rise in the current density is assigned to the breakdown of passive film and the initiation of pitting corrosion.[28] The steady-state current obtained may be due to the competitive balance among the formation of the oxide films, the dissolution of the passive layer and the dissolution of Hf. It is observed that the corrosion current is enhanced with the increase in the Br⁻ concentration, which can be explained by following points: The higher the bulk Br⁻ ion concentration, the higher will be the local Br⁻ ion concentration that is responsible for initiating pit formation at defect areas and enhancing the exposed metal dissolution.
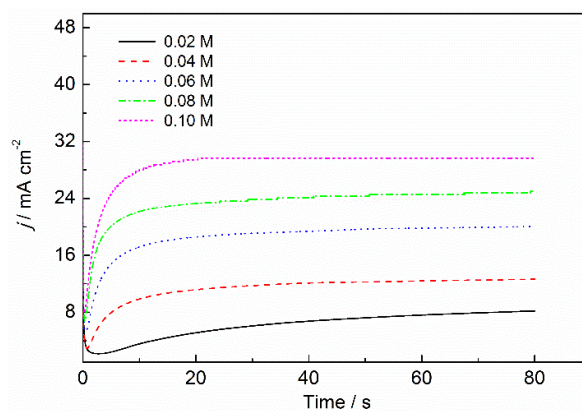

Fig. 6 Current-time transients for Hf in anhydrous ethanol with various Et₄NBr concentrations at a constant step anodic potential of 2.5 V.

Fig. 7 presents characteristic Nyquist diagrams of Hf in anhydrous ethanol with various Et₄NBr concentrations at a constant potential of 2.5 V. It is observed that the capacitive arc decreases significantly with increasing Br⁻ ions concentration from 0.02 M to 0.10 M. Notably, both the capacitive arc and Warburg tail are

found, corresponding to the appearance of the electrochemical control in the high frequency range and a diffusion-controlled process in the low frequency range.[32] This may be due to the high concentration of the corrosion product salt film, which hinders the corrosion current through the hole.[33] As the Br⁻ ions concentration increases, the curve shifts in a more negative direction, and the capacitive arc becomes smaller. However, when the Br⁻ ions concentration attains to a certain value, the trend clearly slows down.
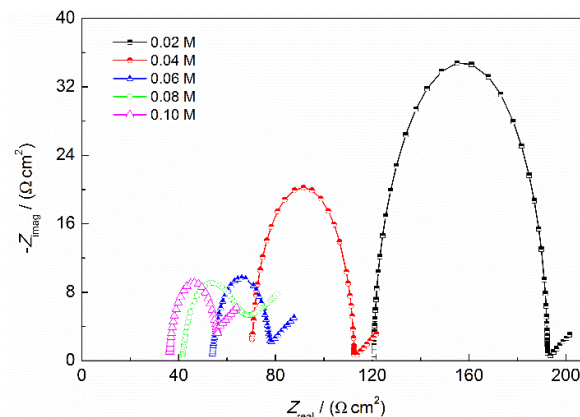

Fig. 7 Nyquist plots of Hf in anhydrous ethanol with various Et₄NBr concentrations at a constant anodic potential of 2.5 V.
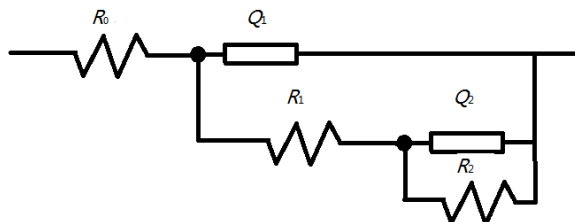

Fig. 8 Equivalent circuit to fit the experimental data for various potentials.

The Nyquist plot shows the time constants and can be modeled using the equivalent circuit presented in Fig. 8, in which R_0 represents the electrolyte resistance, and R_1 and R_2 correspond to the charge transfer resistance and the resistance of the passive layer, respectively. Q_1 is a constant phase element (CPE) related to the double layer capacitance. Q_2 is the capacitance of the passive layer. CPE is a constant phase element used to describe the distribution of the microscopic level by an empirical impedance function of the type:[34]

$$Z = [Q / (jw)^n]^{-1} \qquad\qquad (2)$$

where w is the angular frequency, $j^2 = -1$ is the imaginary number and n is the CPE exponent, which reflects the deviation of the capacitance from the ideal capacitive behavior. The value of -1 is characteristic of an inductance, the value of 1 corresponds to a capacitor, the value of 0 corresponds to a resistor and the value of 0.5 can be assigned to diffusion phenomena. The fitting electrochemical parameters are listed in Table 1. It is observed that R_0, R_1 and R_2 decrease sharply as the Br⁻ ions concentration increases, indicating that a higher Br⁻ concentration can accelerate Hf dissolution in anhydrous ethanol. These can be explained by following points: The breakdown of the passive film and the initiation of the pitting corrosion are due to the ability of Br⁻ ions to adsorb on the passive surface. The adsorption process is followed by the removal of the oxide film, particularly at flaws and defective sites as complex ions, where the oxide films can be totally removed and the base metal exposed to the electrolyte.

The higher the bulk Br⁻ ion concentration is, the higher possibility the adsorption of Br⁻ ions on the passive surface has.

Table 1 Electrochemical parameters obtained by fitting

Concentrations/ M	R_o/ Ω cm^2	Q_1/ Ω^{-1} cm^{-2} s^n	n_1	R_1/ Ω cm^2	Q_2/ Ω^{-1} cm^{-2} s^n	n_2	R_2/ Ω cm^2
0.02	120.7	4.001×10^{-6}	1	72.79	1.949×10^{-5}	1	58.58
0.04	73.14	1.118×10^{-9}	1	70.35	4.932×10^{-6}	0.9721	42.19
0.06	53.72	1.589×10^{-5}	0.842	24.81	3.478×10^{-1}	0.8	22.55
0.08	41.60	1.248×10^{-5}	0.8696	15.29	2.395×10^{-2}	0.8	15.00
0.10	36.13	6.623×10^{-6}	0.9342	10.17	2.707×10^{-2}	0.7868	14.00

3.5 Influence of electrode potential

Fig. 9 displays the potentiostatic current-time transients for Hf in a 0.06 M Et₄NBr solution of anhydrous ethanol at various potentials (E) with a time of 200 s for the experiment. For $E = 0.4$ V, the current density gradually decreases to a stable state value, suggesting that the low potential is not enough to induce pitting corrosion. However, for $E \geq 1.2$ V, the current densities initially decrease to minimum values at a certain incubation time (t_i) and then rise steadily, indicating the breakdown of the passive film by Br⁻ ions and the initiation of the pitting corrosion. With the increase of the electrode potential, t_i decreases slightly, which indicates that the passive film is more prone to be punctured by a higher potential. This can be explained by the following point: The electrode potential can reduce the activation energy of the oxidation reaction but increase the activation energy of the reduction reaction.
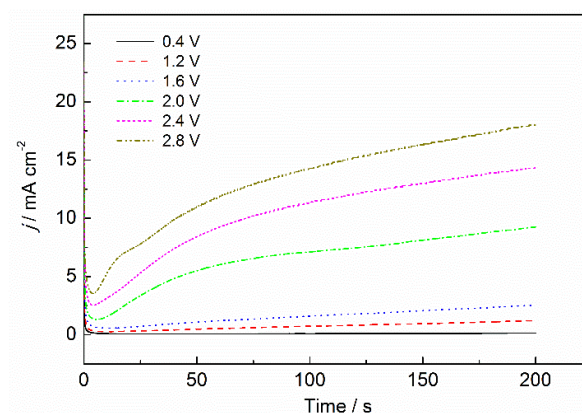

Fig. 9 Potentiostic current-time transients for Hf in 0.06 M Et₄NBr solution of anhydrous ethanol at various potentials: 0.4-2.8 V.

Fig. 10 shows characteristic Nyquist diagrams of Hf in a 0.06 M Et₄NBr solution of anhydrous ethanol at various electrode potentials. It is clear that the capacitive arc decreases significantly with increasing electrode potentials from 0.4 V to 0.8 V. Notably, only capacitive arcs are found, without any sign of Warburg tail. These findings indicates that the electrochemical control has taken place, while the diffusion control has not yet appeared. However, when the potential is higher than 1.2 V, at which point the impedance value is lower than the impedance

value of -4 V by approximately two orders of magnitude, it is observed that the decline clearly slows down, and capacitive arcs in the low frequency range are replaced by Warburg tails, corresponding to the formation of pitting corrosion and the appearance of a diffusion-controlled process at high electrode potentials.[32] This may be due to the high concentration of the corrosion product salt film, which hinders the corrosion current through the hole.[33]
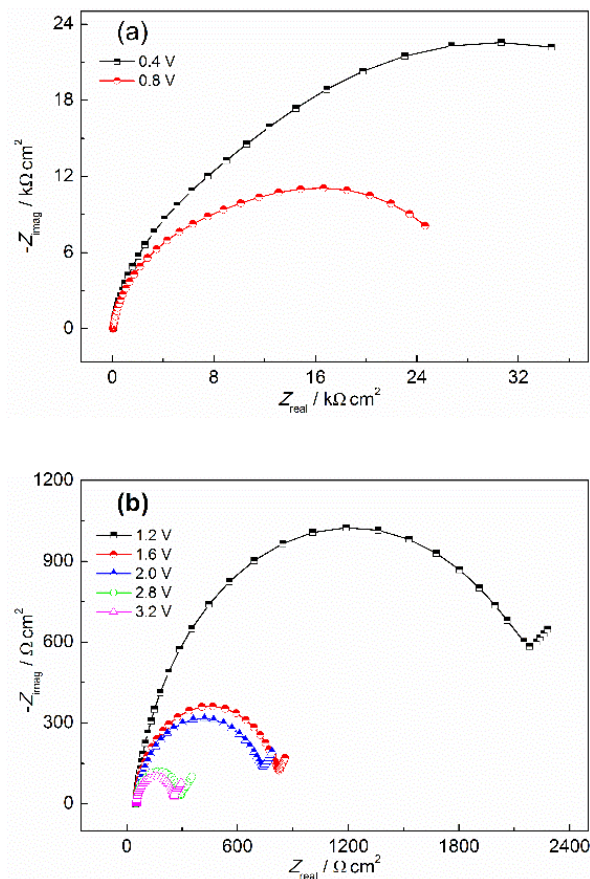

Fig.10 Nyquist plots of Hf in 0.06 M Et₄NBr solution of anhydrous ethanol at various potentials:
(a) -0.4-0.8 V; (b) 1.2-3.2 V.

The Nyquist plot shows the time constants and can be modeled using the equivalent circuit presented in Fig. 8. The fitting electrochemical parameters are listed in Table 2. It is observed that the values of R_0 are nearly constants, while R_1 and R_2 decrease sharply as the electrode potential increases, indicating that a higher potential can accelerate the dissolution of the passive film and Hf in anhydrous ethanol.

Table 2 Electrochemical parameters obtained by fitting

Potential/ V	R_o/ Ω cm^2	Q_1/ Ω^{-1} cm^{-2} s^n	n_1/	R_1/ Ω cm^2	Q_2/ Ω^{-1} cm^{-2} s^n	n_2/	R_2/ Ω cm^2
0.4	47.72	1.22×10^{-5}	0.9144	29800	2.681×10^{-5}	0.8	25200
0.8	48.15	1.14×10^{-5}	0.9114	19480	4.659×10^{-5}	1	9340
1.2	48.66	9.751×10^{-6}	0.9211	2315	4.424×10^{-6}	1	2174
1.6	50.68	8.291×10^{-6}	0.9392	796.7	1.101×10^{-3}	0.796	1084

2.0	50.90	8.924×10^{-6}	0.9168	720.4	6.651×10^{-3}	1	963
2.8	51.27	5.41×10^{-6}	0.9818	246.4	1.086×10^{-3}	1	529
3.2	51.43	5.317×10^{-6}	0.9833	207.8	1.191×10^{-4}	1	491

3.6 SEM microphotographs of hafnium surface after corrosion

Fig. 11 presents SEM microphotographs of the Hf surface after anodization at 2.5 V for 3 min in anhydrous ethanol containing various Et_4NBr concentrations (C). As displayed in Fig. 11, no pitting phenomena occur on the specimen after polishing, but only the traces of polish exist on it, as in image A. On the contrary, SEM observations reveal the occurrence of intense pitting corrosion on the specimen exposed to the test solution, as in images B, C and D. The concentration increase results in deeper and more defined pits (compare among images B, C and D). It is observed that the corrosion of hafnium occurs through pitting rather than uniform corrosion. This may be due to the natural immediate formation of an electrically insulating inert and stable passive layer on the Hf surface. Therefore, by SEM, can we clearly see the growth of the pitting process, further confirming the existence of pitting corrosion after anodization in anhydrous ethanol solution containing Br^- ions.
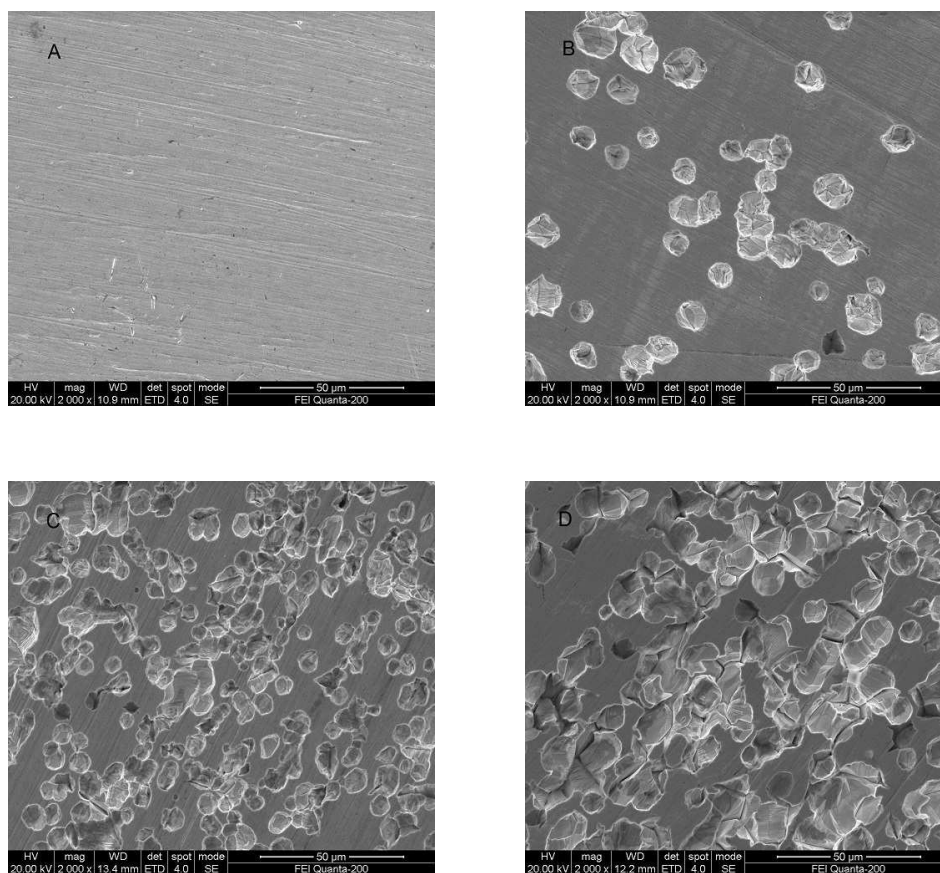

Fig. 11 SEM microphotographs of Hf surface after anodization at 2.5 V for 3 min in anhydrous ethanol containing various Et_4NBr concentrations: (a) after polishing; (b) 0.02 M; (c) 0.06 M; (d) 0.10 M.

4. Conclusions

Investigations of the electrochemical behaviors of Hf in Et_4NBr ethanol solutions were performed by means

of cyclic voltammetry, potentiodynamic polarization, chronoamperometry, impedance and SEM microphotograph techniques. Results show that when the surface of Hf is subjected to a certain anodic potential, a hysteresis loop is clearly observed in cyclic voltammetry, a crucial characteristic of the pitting corrosion phenomenon. The anodic excursion span does not exhibit an active dissolution due to the presence of an oxide film on the electrode surface, which is followed by pitting corrosion as a result of the passivity breakdown by the aggressive attack of Br^-. The pitting potential (E_b) shifts to more noble values with increasing scanning rate, but in a more negative direction with increasing solution temperature and Br^- concentration. The apparent activation energy is calculated as 27.074 kJ mol^{-1} by the Tafel extrapolation. An anodic current peak is observed in the flyback curve of the cyclic voltammogram. The potentiostatic current–time transients reveal that the current density gradually decreases to a stable state value when the applied potential is low; however, the current density initially decreases to a minimum value at a certain incubation time (t_i), and then rises to a steady-state value when the potential is higher than a certain value. t_i for passivity breakdown decreases with increasing applied positive potential and Br^- concentration. The impedance spectra exhibits that the resistance of the passive layer and charge transfer decreases with an increase in the Br^- concentration and applied positive potential, while the resistance of solution is nearly constant with increasing applied positive potential and decreases with increasing Br^- concentration. The Hf surface morphology and the growth of the pitting process are studied by SEM and its images confirmed the existence of pitting corrosion on the Hf surface.

Acknowledgments

References

[1] G. E. Moore, *Electrics*, 1965, 38, 114-116.

[2] E. Hildebrandt, J. Kurian, J. Zimmermann, A. Fleissner, H. von Seggern and L. Alff, *American Vacuum Society*, 2009, 27, 325-327.

[3] M. Ieong, B. Doris, J. Kedzierski, K. Rim and M. Yang, *Science*, 2004, 306, 2057-2060.

[4] B. Yu, H. Wang, C. Riccobene, Q. Xiang, and M. –R. Lin, *Dig. Tech. Pap. Symp. VLSI Technol.* 2000, 24, 90.

[5] J. H. Choi, Y. Mao and J. P. Chang, *Materials Science and Engineering R*, 2011, 72, 98-100.

[6] M. T. Bohr, R. S. Chau, T. Ghani and K. Mistry, *IEEE Spectrum*, 2007, 44, 29-31.

[7] D. H. Hill, R. A. Bartynski, N. V. Nguyen and A. C. Davydov, *Journal of Applied Physics*, 2008, 103, 93-101.

[8] J. Niinistö, K. Kukli, T. Sajavaara, M. Ritala, M. Leskelä, L. Oberbeck, J. Sundqvist and U. Schröder, *Electrochemical and Solid-State Letters*, 2009, 12, 1-4.

[9] S. Dueñas, H. Castán, H. Garcia, A. Gómez, L. Bailón，K. Kukli，J. Niinistö, M. Ritala and M. Leskelä, *Journal of Vacuum Science & Technology B*, 2009, 27, 389-393.

[10] C. L. Dezelah, J. Niinistö, K. Kukli, F. Munnik, J. Lu, M. Ritala, M. Leskelä and L. Niinistö, *Chemical Vapor Deposition*, 2008, 14, 358–365.

[11] J. C. Kim, J. S. Heo, Y. S. Cho and S. H. Moon, *Thin Solid Films*, 2009, 517, 5695-5699.

[12] E. Rauwel, F. Ducroquet, P. Rauwel, M. -G. Willinger, I. Matko and N. Pinna, *Journal of Vacuum Science & Technology B: Microelectronics and Nanometer Structures*, 2009, 27, 230-235.

[13] K. Xu, A. P. Milanov, M. Winter, D. Barreca, A. Gasparotto, H-. W. Becker and A. Devi, *European Journal of Inorganic Chemistry*, 2010, 2010, 1679-1688.

[14] K. Reuter, F. Zell and M. Ebner, US 7,273, 2007, 943.

[15] V. A. Shreider, E. P. Turevskaya, N. I. Koslova and N. Y. Turova, *Inorganica Chimica Acta*, 1981, 53, 73-76.

[16] S. H. Yang, Y. M. Chen, H. P. Yang, Y. Y. Liu, M. T. Tang and Z. Z. Qiu, *Transactions of Nonferrous Metals Society of China*, 2008, 18, 196-201.

[17] E. P. Turevskaya, N. I. Kozlova, N. Y. Turova, A. I. Belokon, D. V. Berdyev, V. G. Kessler and Y. K. Grishin, *Russian Chemical Bulletin*, 1995, 44, 734-742.

[18] M. Y. Berezkin, I. N. Chernykh, E. G. Polyakov and A. P. Tomilov, *Applied Electrochemistry and Corrosion Protection of Metals*, 2006, 79, 752-756.

[19] A. D. Davydov, *Electrochimica Acta*, 2001, 46, 3777-3781.

[20] M. Berezkin, E. Polyakov, V. Turygin and A. Tomilov, *Russian Journal of Electrochemistry*, 2007, 43, 1200-1202.

[21] H. P. Yang, S. H. Yang, Y. N. Cai, G. F. Hou and M. T. Tang, *Electrochimica Acta*, 2010, 55, 2829-2834.

[22] M. Kutz, *Hand Book of Environmental Degradation of Materials*, William, Andrew, USA, 2nd edn., 2012.

[23] E. E. Stansbury and R. A. Buchanan, *Fundamentals of Electrochemical Corrosion*, ASM International, USA, 2000.

[24] H. Kaesehe, *Materials and Corrosion*, 1988, 39, 153-161.

[25] S. B. Han, Y. J. Song, J. M. Lee, J. Y. Kim and K. W. Park, *Electrochemistry Communication*, 2008, 10, 1044-1047.

[26] M. A. Amin and S. S. Abdel Rehim, *Electrochimica Acta*, 2004, 49, 2415-2424.

[27] H. H. Hassan, *Electrochimica Acta*, 2005, 51, 526-535.

[28] S. S. Abd EI Rehim, E. E. Foad EI-Sherbini and M. A. Amin, *Journal of Electroanalytical Chemistry*, 2003, 560, 175-182.

[29] J. J. Park and S. I. Pyun, *Corrosion Science*, 2003, 45, 995-1010.

[30] M. A. M. Ibrahim, S. S. Abd EI Rehim and M. M. Hamza, *Materials Chemistry and Physics*, 2009, 115, 80-85.

[31] H. H. Hassan and K. Fahmy, *International Journal of Electrochemical Science*, 2008, 3, 29-43.

[32] A. J. Bard and L. R. Faulkner, *Electrochemical Methods: Fundamentals and Applications*, John Wiley & Sons, Inc., New York, 2001.

[33] M. A. Amin, S. S. Abd EI-Rehim, E. E. F. EI-Sherbini, S. R. Mahmoud and M. N. Abbas, *Electrochemica Acta*, 2009, 54, 4288-4296.

[34] A. H. Moreira, A. V. Benedetti, P. T. A. Sumodjo, J. A. Garrido and P. L. Cabot, *Electrochimica Acta*, 2002, 47, 2823-2831.